Article

Discovery Medicine 2025; 37(200): 1849–1859
https://doi.org/10.24976/Discov.Med.202537200.160

Trefoil Factor 3 Knockdown Promotes Autophagy and Mitigates Cardiac Hypertrophy and Fibrosis via the CXCR4/JAK/STAT Signaling Pathway

Juan Liu[1,†], Yongsheng Li[1,†], Zhongcheng Wei[2,*], Hailang Liu[2]

[1]Department of Rheumatology, The Affiliated Huai'an No.1 People's Hospital of Nanjing Medical University, 223300 Huai'an, Jiangsu, China
[2]Department of Cardiology, The Affiliated Huai'an No.1 People's Hospital of Nanjing Medical University, 223300 Huai'an, Jiangsu, China
*Correspondence: weicheng060@126.com (Zhongcheng Wei)
[†]These authors contributed equally.
Submitted: 24 April 2025 Revised: 31 July 2025 Accepted: 15 August 2025 Published: 20 September 2025

Background: Heart failure (HF) remains a leading cause of morbidity and mortality worldwide, characterized by cardiac hypertrophy, fibrosis, and impaired function. Despite advances in therapeutic strategies, novel molecular targets are urgently needed to improve clinical outcomes. Trefoil factor 3 (Tff3) is reported to be upregulated in patients with heart failure. However, its functional role and underlying mechanisms in disease progression remain unclear. This study aimed to investigate the role of Tff3 in heart failure progression *in vivo* and to elucidate its molecular mechanisms.

Methods: A mouse model of heart failure was established via thoracic aortic coarctation (TAC). Tff3 expression in cardiac tissue was evaluated using immunoblotting and immunohistochemistry. Cardiac hypertrophy and fibrosis were assessed by immunoblotting, Masson's trichrome staining, and wheat germ agglutinin (WGA) staining. Autophagy levels were determined through immunoblotting and immunostaining. The involvement of the C-X-C Chemokine Receptor Type 4 (CXCR4)/Janus Kinase (JAK)/Signal Transducer and Activator of Transcription (STAT) signaling pathway was examined by immunoblot analysis.

Results: Tff3 expression was significantly upregulated in heart failure models ($p < 0.05$). Knockdown of Tff3 alleviated TAC-induced cardiac hypertrophy and fibrosis ($p < 0.05$). Furthermore, Tff3 depletion enhanced autophagy in heart failure models ($p < 0.05$). Mechanistically, Tff3 knockdown suppressed activation of the CXCR4/JAK/STAT signaling axis in heart failure mice ($p < 0.05$). These findings suggest that Tff3 depletion mitigates heart failure progression through the CXCR4/JAK/STAT axis ($p < 0.05$).

Conclusion: Tff3 knockdown promotes autophagy and attenuates cardiac hypertrophy and fibrosis by regulating the CXCR4/JAK/STAT signaling pathway. Tff3 may serve as a promising therapeutic target for heart failure.

Keywords: heart failure; cardiac fibrosis; trefoil factor 3; cardiac hypertrophy; CXCR4/JAK/STAT pathway

Introduction

Cardiovascular diseases (CVDs) remain the leading cause of mortality worldwide, accounting for approximately 32% of all deaths (18.6 million annually), as reported by the World Health Organization. Ischemic heart disease alone is responsible for 16% of total deaths, with heart failure (HF) constituting a major contributor to this global health burden. HF is among the most prevalent and life-threatening chronic conditions worldwide. It is a complex and progressive clinical syndrome characterized by the heart's inability to pump sufficient blood to meet the metabolic demands of peripheral tissues and organs [1]. The condition may result from diverse etiologies, including infections, hypertension, myocardial infarction, chronic ischemia, and pathological hypertrophy [2].

A hallmark of HF is maladaptive cardiac remodeling, characterized by interstitial fibrosis, ventricular remodeling, and reduced ventricular compliance. This process is driven by activated cardiac fibroblasts, which mediate excessive deposition of extracellular matrix (ECM) proteins such as type I collagen and fibronectin. Cardiac fibroblast activation is recognized as a major factor in HF progression [3]. Despite significant advances in pharmacological interventions and device-based therapies, HF presents significant clinical challenges, underscoring the urgent need for novel molecular targets to improve patient outcomes and reduce disease burden.

Trefoil factor 3 (Tff3) is a 6 kDa secreted protein belonging to the trefoil factor family (Tff), which also includes Tff1 and Tff2. Members of this family are defined by at least one trefoil domain, a conserved 40-amino-acid motif containing three intrachain disulfide bonds that stabilize a distinctive three-loop (trilobal) structure [4]. Tff3 plays an essential role in the maintenance and repair of mucosal tissues by promoting epithelial cell migration during the

healing process and functioning as a mitogen [5]. Although it primarily exists as a monomer, Tff3 can form disulfide-linked homodimers, suggesting potential roles in protein-protein interactions and modulation of signaling cascades [6].

The role of Tff3 in mucosal repair underscores its importance in dynamic processes that preserve epithelial integrity and barrier function [7]. Elevated Tff3 expression has been reported in patients with HF compared to healthy controls, suggesting a potential role in cardiovascular pathology [8]. Beyond the cardiovascular system, Tff3 deficiency has been shown to prevent hepatic steatosis following chronic high-fat diet exposure and to regulate immune responses by modulating the NF-κB/COX2 pathway in polymorphonuclear myeloid-derived suppressor cells (PMN-MDSCs), thereby preventing necrotizing enterocolitis [9]. Furthermore, Tff3 overexpression has been implicated in the progression of prostate cancer by inhibiting mitochondria-mediated apoptosis [10]. However, the specific role and mechanisms of Tff3 in HF pathogenesis remain unclear and require further investigation.

In this study, we demonstrate that Tff3 expression is markedly upregulated in a murine model of HF. Genetic knockdown of Tff3 enhanced autophagy and reduced pathological cardiac hypertrophy and fibrosis, primarily via regulation of the CXCR4/JAK/STAT signaling pathway. These findings provide mechanistic evidence supporting Tff3 as a pathogenic mediator in HF and suggest that targeting Tff3 may serve as a promising therapeutic strategy for mitigating disease progression.

Materials and Methods

Animal Models

All animal experiments were approved by the Ethics Committee of The Affiliated Huai'an No.1 People's Hospital of Nanjing Medical University (Approval No. 2023-117) and conducted in accordance with institutional and national guidelines for the care and use of laboratory animals. Male C57BL/6 mice, 8 weeks old, were obtained from Vital River Laboratory Animal Technology Co., Ltd. (Beijing, China) and maintained under specific pathogen-free (SPF) conditions with controlled temperature (20 °C), humidity (40%–60%), and a 12-hour light/dark cycle. Standard food and water were provided *ad libitum*.

Thoracic Aortic Constriction (TAC) Model

Pressure overload-induced HF was established using the thoracic aortic constriction (TAC) model, following a previously described protocol with minor modifications [2]. This method is based on a widely recognized surgical approach and was not originally developed in our laboratory. Briefly, 8-week-old male C57BL/6 mice were anesthetized with 2% isoflurane via inhalation. A total of 40 mice were randomly assigned to five groups (n = 8 per group) using a random number table: Sham group: Sham-operated mice without aortic constriction; Sham + Tff3 knockout (Tff3 KO) group: Sham-operated mice with Tff3 knockout; HF group: Mice subjected to TAC surgery; HF + NC group: TAC mice injected with a control adenovirus (non-targeting sgRNA); HF + Tff3 KO group: TAC mice with Tff3 knockout.

Randomization was performed after confirming successful TAC induction (7 days post-surgery) to ensure uniform distribution of baseline characteristics. Mice failing to meet modeling criteria or dying post-surgery (n = 2) were excluded. For euthanasia, mice were placed in an induction chamber and exposed to 5% isoflurane (vol/vol) in 100% oxygen at a flow rate of 1–2 L/min until loss of consciousness (typically within 2–3 minutes). Death was confirmed by cervical dislocation following cessation of breathing and absence of pedal reflex.

Surgery was performed via a longitudinal incision at the level of the second intercostal space to expose the aortic arch. A 7-0 silk suture was positioned around the transverse aorta alongside a 27-gauge blunt needle placed parallel to the vessel. The suture was tied securely, after which the needle was removed to create a fixed constriction. Sham-operated mice underwent an identical procedure without aorta ligation.

Model success was confirmed 7 days post-surgery by echocardiography, demonstrating increased peak flow velocity across the constriction site (>4.5 m/s), indicative of effective pressure overload. The development of cardiac hypertrophy and fibrosis was further verified by heart weight/body weight ratio, histological analysis with Masson's trichrome staining, and molecular detection of fibrosis-related markers. Sham-operated mice underwent the same procedure without the aortic constriction. Mice that failed to survive or did not meet modeling success criteria were excluded from further analysis. Mice were euthanized 4 weeks after TAC surgery by overdose of isoflurane inhalation, followed by cervical dislocation. Cardiac tissues were immediately harvested and processed for protein extraction, RNA isolation, histological staining, and immunostaining.

Generation of Tff3 and CXCR4 Knockout Mice

Tff3 knockout (*Tff3* KO) mice were generated via adenovirus-mediated CRISPR/Cas9 gene editing. Recombinant adenoviruses expressing Cas9 and a single guide RNA (sgRNA) targeting Tff3 were designed and constructed by Heyuan Biotechnology (Shanghai, China). The sgRNA sequence was selected using the CRISPR design tool to minimize predicted off-target effects. The sgRNA was cloned into a px459-based vector carrying the Cas9 nuclease under a CMV promoter. For Tff3 knockout, sgRNAs targeting exons were co-injected with Cas9 mRNA into C57BL/6 zygotes. The sgRNA sequence was shown as follows: Exon 1 sgRNA-1:

5′-GACATGGCTCTGAGCCAGCA-3′; sgRNA-2: 5′-GCCAGCATGCTGCTGCTGGG-3′.

For CXCR4 overexpression (OE), wild-type mice received tail vein injections of adenovirus carrying full-length CXCR4 cDNA (1×10^{11} viral particles/mouse). Control mice were injected with a non-targeting adenovirus. Overexpression efficiency was verified by qPCR and Western blot analysis 7 days post-injection. The experimental groups included: (1) Tff3 KO mice subjected to TAC, (2) wild-type mice with CXCR4 OE subjected to TAC, and (3) Tff3 KO mice administered CXCR4 OE adenovirus after TAC surgery, in addition to the corresponding control groups (Sham, Sham + Tff3 KO, HF, HF + NC) as previously above. All genetic manipulations and experimental procedures included appropriate controls to ensure the validity of intergroup comparisons.

Knockout success was verified by Sanger sequencing of tail DNA at weaning (3 weeks) and by Western blot analysis at 8 weeks, with survival rates of 85–87% post-injection (Tff3 KO: n = 15; Cxcr4 OE: n = 15). For TAC experiments, mice were grouped into wild-type (WT) controls (n = 12), KO models (n = 15/group), and adenoviral CXCR4 OE (n = 18), with exclusions for failed genotyping (n = 3) or post-surgical mortality (n = 6). All mice were euthanized at 12 weeks of age (or 4 weeks post-TAC) via 5% isoflurane overdose, followed by cervical dislocation. Hearts, blood, and lung/liver tissues were collected for Western blotting, histological evaluation, and fibrosis analysis. For *in vivo* gene editing, adenovirus was administered via tail vein injection at a dose of 1×10^{11} viral particles/mL (100 µL per mouse). Control animals received a non-targeting sgRNA adenovirus.

Immunoblot Analysis

Cardiac tissues were homogenized, and total proteins were extracted using RIPA buffer (Beyotime, P0013B, Shanghai, China). Protein concentrations were quantified with the BCA Protein Assay Kit (Beyotime, P0010). Equal amounts of protein (30 µg) were resolved by SDS-PAGE and transferred to PVDF membranes. Membranes were blocked with 5% non-fat milk in TBST for 1 hour, then incubated overnight at 4 °C with primary antibodies from Abcam (Cambridge, UK): Tff3 (ab300427, 1:1000), GAPDH (ab9485, 1:5000), LC3B (ab192890, 1:1000); P62 (ab109012, 1:1000), CXCR4 (ab124824, 1:1000), JAK2 (ab108596, 1:1000), p-JAK2 (ab32101, 1:1000), STAT3 (ab68153, 1:1000), p-STAT3 (ab32143, 1:1000), ANP (ab225844, 1:1000), BNP (ab309127, 1:1000), Collagen I (ab270993, 1:1000), and α-SMA (ab124964, 1:1000). Membranes were then washed and incubated with HRP-conjugated secondary antibodies goat anti-rabbit IgG H&L (HRP) (Abcam, ab6721, 1:5000) for 1 hour at room temperature. Protein bands were visualized using an ECL detection kit (Beyotime, P0018S).

Western blot images were acquired with the Tanon 5200 Multi Chemiluminescent Imaging System (Tanon, Shanghai, China). Image quantification was performed using ImageJ software (NIH, Bethesda, MA, USA).

Immunohistochemical (IHC) and Immunofluorescence Staining

Histological specimens were prepared from formalin-fixed, paraffin-embedded mouse heart tissues collected 4 weeks post-TAC. Hearts were excised, rinsed in PBS, fixed in 4% paraformaldehyde overnight at 4 °C, and embedded in paraffin. Tissue sections of 5 µm thickness were obtained using a microtome (Leica RM2016) and mounted on glass slides for staining. For immunohistochemistry, sections were deparaffinized, rehydrated, and subjected to antigen retrieval by boiling in citrate buffer (pH 6.0). Following blocking with 5% BSA, sections were incubated overnight at 4 °C with a primary antibody against Tff3 (ab300427, 1:200, Abcam). After washing, sections were incubated with HRP-conjugated secondary antibodies (ab6721, 1:200, Abcam), and staining was visualized using DAB substrate (Beyotime, P0203). Quantitative analysis of immunohistochemical staining was performed using ImageJ software (NIH, USA). The integrated optical density (IOD) was determined by multiplying the stained area by the mean optical density after background subtraction.

For immunofluorescence, sections were blocked with 5% BSA and incubated overnight at 4 °C with primary antibody against LC3B (ab192890, 1:200, Abcam). Subsequently, sections were incubated with fluorescently labeled secondary antibodies (Goat anti-Rabbit IgG (H+L) Cross-Adsorbed Secondary Antibody, Alexa Fluor 488, Thermo Fisher Scientific, A-11008, 1:500) and counterstained with DAPI (Beyotime, C1006). Fluorescence images were captured using a Zeiss fluorescence microscope (LSM710) under identical exposure settings for all samples.

Histological Analysis

Masson's trichrome staining was performed to evaluate cardiac fibrosis. Cardiac sections were processed using a Masson's Trichrome Stain Kit (Beyotime, C0189M) following the manufacturer's instructions. The fibrotic area was quantified using ImageJ by thresholding Masson's trichrome-stained sections from 6 mice per group. Values were normalized to the total myocardial area and expressed as percentage fibrosis (mean ± SD).

Wheat germ agglutinin (WGA) staining was used to determine cardiomyocyte cross-sectional area. Sections were incubated with WGA conjugated to Alexa Fluor 488 (Thermo Fisher Scientific, W11261, 1:200) and imaged. Images of Masson's trichrome- and WGA-stained sections were acquired using a Zeiss Axio Imager M2 microscope (Carl Zeiss AG, Germany) equipped with an Axiocam 506 color camera (Zeiss) and ZEN 2.3 imaging software (Zeiss). For fluorescence imaging (WGA staining), the mi-

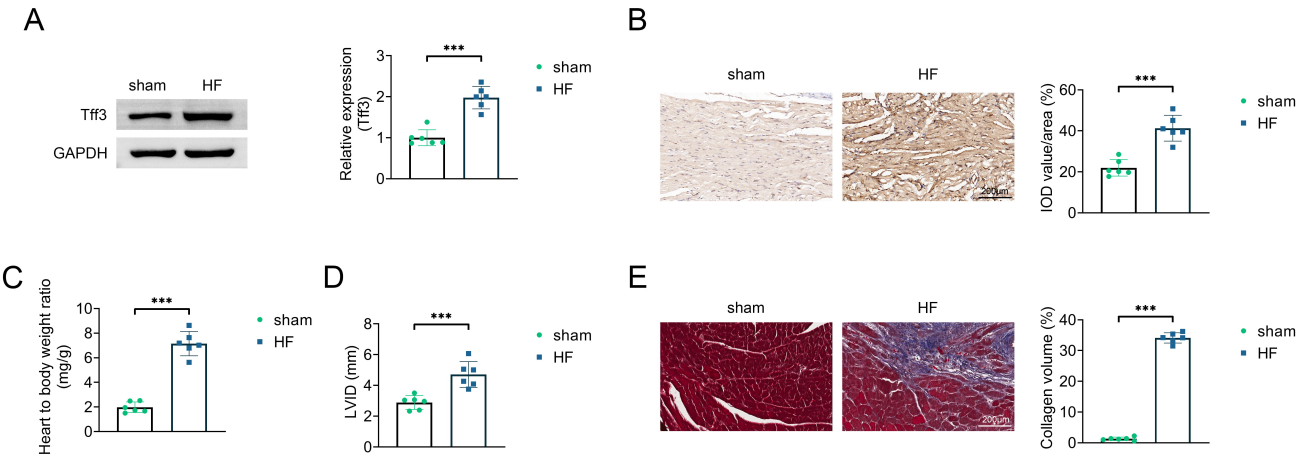

Fig. 1. Trefoil factor 3 (Tff3) is upregulated in experimental heart failure models. (A) Immunoblot analysis of Tff3 expression in sham and heart failure (HF) groups. Quantification of relative Tff3 expression is shown on the right. (B) Immunohistochemical staining of cardiac tissue sections from sham and HF groups, demonstrating increased Tff3 expression in HF (quantified by integrated optical density (IOD) values). (C) Heart-to-body weight ratio of mice in the sham and HF groups. (D) Left ventricular internal diameter (LVID) in sham and HF groups. (E) Masson's trichrome staining of cardiac tissue sections showing collagen deposition in sham and HF groups (scale bar = 200 µm). n = 6 per group. Data are presented as mean ± standard deviation (SD). ***$p < 0.001$.

croscope was configured with appropriate filter sets (excitation/emission: 488/519 nm for Alexa Fluor 488). All images were captured under identical illumination conditions using a 20× objective (NA 0.8), with exposure times optimized for each staining protocol and maintained constant across samples within the same experiment. Cardiomyocytes' cross-sectional areas were quantified using ImageJ software.

Statistical Analysis

All data are presented as mean ± standard deviation (SD). Data normality was assessed using the Shapiro-Wilk test, and homogeneity of variances was evaluated using Levene's test. Comparisons between two groups were performed using an unpaired, two-tailed Student's *t*-test. For comparisons across multiple groups, one-way ANOVA followed by Tukey's post hoc test was applied. Statistical analyses were conducted using GraphPad Prism version 9.0 (GraphPad Software, San Diego, CA, USA). A p-value < 0.05 was considered statistically significant.

Results

Tff3 Is Upregulated in Heart Failure Models

To investigate the role of Tff3 in HF, we first examined its expression in a murine HF model induced by thoracic aortic constriction (TAC). Immunoblotting revealed a significant upregulation of Tff3 in HF group compared to sham group ($p < 0.05$) (Fig. 1A). Immunohistochemistry further confirmed elevated Tff3 expression in myocardial tissue sections from TAC group (Fig. 1B). Successful establishment of the HF model was validated by a significant increase in the heart weight-to-body weight (HW/BW) ratio and an enlargement of the left ventricular end-systolic diameter (LVIDs) in TAC group (Fig. 1C,D). Additionally, Masson's trichrome staining revealed a marked increase in myocardial fibrosis in TAC group compared to sham group (Fig. 1E). Collectively, these results demonstrate that Tff3 is upregulated in pressure overload-induced HF and supports its potential role in HF pathogenesis.

Tff3 Depletion Reduces TAC-induced Cardiac Hypertrophy and Fibrosis

To determine the functional role of Tff3 in HF, we generated Tff3 knockout (Tff3 KO) mice and examined the effects on cardiac hypertrophy and fibrosis. Immunoblotting confirmed the successful knockout of Tff3 in HF + Tff3 KO group ($p < 0.05$) (Fig. 2A). The HW/BW ratio, an established marker of cardiac hypertrophy, was significantly reduced in HF + Tff3 KO group compared to HF + NC group ($p < 0.05$) (Fig. 2B). Additionally, the left ventricular internal diameter (LVID) was significantly decreased in HF + Tff3 KO group ($p < 0.05$) (Fig. 2C). Masson's trichrome staining revealed attenuated myocardial fibrosis in HF + Tff3 KO group ($p < 0.05$) (Fig. 2D), while wheat germ agglutinin (WGA) staining indicated a reduction in cardiomyocyte cross-sectional area ($p < 0.05$) (Fig. 2E). Furthermore, immunoblotting revealed reduced expression of ANP, BNP, collagen I, and α-SMA in HF + Tff3 KO group (Fig. 2F). These findings indicate that Tff3 deficiency alleviates TAC-induced cardiac hypertrophy and fibrosis, suggesting a detrimental role of Tff3 in HF pathogenesis.

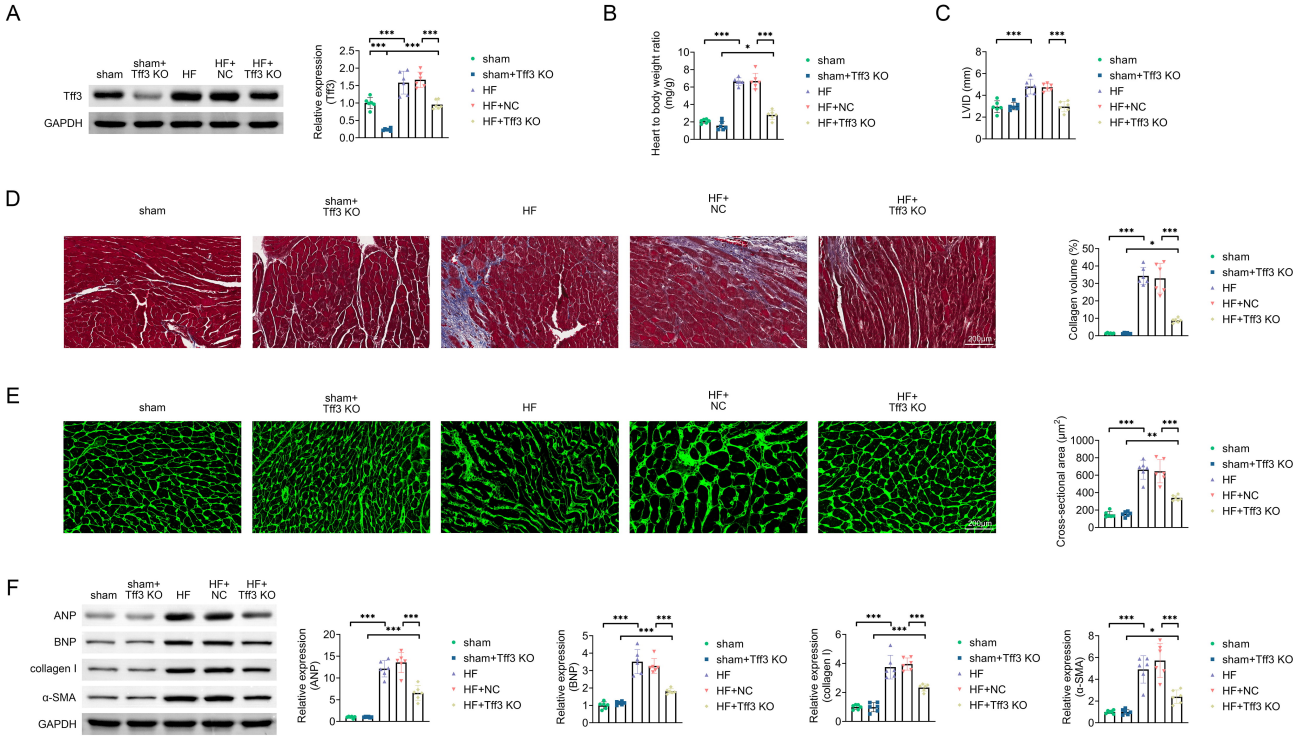

Fig. 2. Tff3 knockout attenuates thoracic aortic constriction (TAC)-induced cardiac hypertrophy and fibrosis. (A) Immunoblot analysis of Tff3 expression in sham, sham + Tff3 knockout (Tff3 KO), HF, HF + NC, and HF + Tff3 KO groups. (B) Heart-to-body weight ratio in sham, sham + Tff3 KO, HF, HF + NC, and HF + Tff3 KO groups. (C) Left ventricular internal diameter (LVID) in sham, sham + Tff3 KO, HF, HF + NC, and HF + Tff3 KO groups. (D) Masson's trichrome staining of cardiac tissue sections from sham, sham + Tff3 KO, HF, HF + NC, and HF+Tff3 KO groups, showing reduced fibrosis in the HF + Tff3 KO group (scale bar = 200 μm). (E) Wheat germ agglutinin (WGA) staining of cardiac tissue sections from sham, sham + Tff3 KO, HF, HF+NC, and HF + Tff3 KO groups, showing reduced cardiomyocyte cross-sectional area in the HF + Tff3 KO group (scale bar = 200 μm). (F) Immunoblot analysis of expression levels of hypertrophy- and fibrosis-associated markers (ANP, BNP, collagen I, and α-SMA) in sham, sham + Tff3 KO, HF, HF + NC, and HF + Tff3 KO groups. n = 6 per group. Data are presented as mean ± SD. *$p < 0.05$, **$p < 0.01$, ***$p < 0.001$. Abbreviations: NC, negative control; KO, knockout.

Knockdown of Tff3 Promotes Autophagy in Heart Failure Models

We next investigated the impact of Tff3 knockout on autophagy in HF models. Immunoblot analysis showed increased LC3-II levels and decreased P62 levels in HF + Tff3 KO group compared to HF + NC group, indicating enhanced autophagy ($p < 0.05$) (Fig. 3A). Immunofluorescence staining for LC3B further demonstrated a marked increase in LC3B-positive puncta in HF + Tff3 KO group (Fig. 3B,C), consistent with elevated autophagosome formation. These findings suggest that Tff3 knockout promotes autophagy in HF models.

Silencing of Tff3 Modulates the CXCR4/JAK/STAT Signaling Pathway

To investigate the molecular mechanism underlying the protective effects of Tff3 knockout in HF, we examined the CXCR4/JAK/STAT signaling pathway. Immunoblot analysis demonstrated that Tff3 knockout in HF group (HF + Tff3 KO) led to decreased CXCR4 expression, accompanied by significantly reduced phosphorylation of JAK2 and STAT3 compared to HF + NC group ($p < 0.05$) (Fig. 4). These findings suggest that Tff3 depletion suppresses activation of the CXCR4/JAK/STAT signaling pathway in HF models.

Knockdown of Tff3 Exerts Cardioprotective Effects Through Regulation of the CXCR4/JAK/STAT Pathway

The role of the CXCR4/JAK/STAT signaling pathway in mediating the protective effects of Tff3 knockout was examined by overexpressing CXCR4 in Tff3-deficient HF mice (HF + Tff3 KO + CXCR4 OE). Immunoblot analysis showed elevated CXCR4 expression, while phosphorylation of JAK and STAT3 was also significantly increased in the HF + Tff3 KO + CXCR4 OE group ($p < 0.05$) (Fig. 5A). The HW/BW ratio and LVID were significantly higher in HF + Tff3 KO + CXCR4 OE group compared to HF + Tff3 KO groups ($p < 0.05$) (Fig. 5B,C). Masson's trichrome staining and WGA staining revealed a further in-

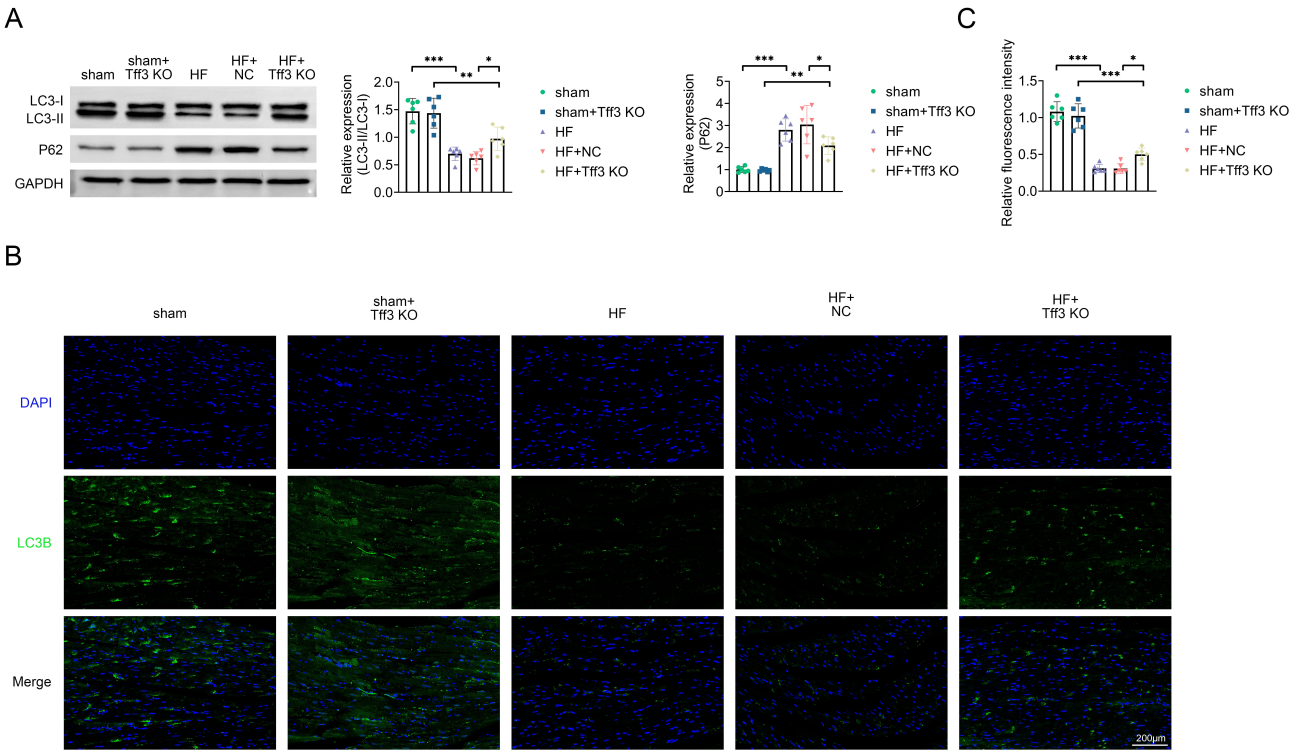

Fig. 3. Tff3 knockdown enhances autophagy in heart failure models. (A) Immunoblot analysis of autophagy-related proteins LC3-I, LC3-II, and P62 in sham, sham + Tff3 KO, HF, HF + NC, and HF + Tff3 KO groups. Quantification of relative LC3-II/LC3-I and P62 expression levels is shown on the right. (B) Immunofluorescence staining of LC3B (green) with DAPI nuclear counterstain (blue) in cardiac tissue sections from sham, sham + Tff3 KO, HF, HF + NC, and HF + Tff3 KO groups, showing increased LC3B puncta in the HF + Tff3 KO group (scale bar = 200 μm). (C) Quantification of LC3B puncta from panel (B). n = 6 per group. Data are presented as mean ± SD. *$p < 0.05$, **$p < 0.01$, ***$p < 0.001$. Abbreviations: NC, negative control; KO, knockout.

crease in fibrosis and cardiomyocyte cross-sectional area in the HF + Tff3 KO + CXCR4 OE group (Fig. 5D,E). Immunoblot analysis of ANP, BNP, collagen I, and α-SMA levels also showed a significant increase in the HF + Tff3 KO + CXCR4 OE group ($p < 0.05$) (Fig. 5F). Furthermore, immunoblot analysis of LC3-I, LC3-II, and P62, along with immunofluorescence staining of LC3B, confirmed suppressed autophagy in the HF + Tff3 KO + CXCR4 OE group ($p < 0.05$) (Fig. 5G,H). Collectively, these findings indicate that the cardioprotective effects of Tff3 knockout in HF are mediated through regulation of the CXCR4/JAK/STAT signaling axis.

Discussion

Heart failure (HF) is a multifaceted and progressive clinical syndrome characterized by the heart's inability to pump adequate blood to satisfy the metabolic demands of the body [11]. The progression of HF involves complex pathophysiological alterations, including myocardial hypertrophy, fibrosis, and impaired contractile performance, all contributing to adverse cardiac remodeling and functional decline [12]. The thoracic aortic constriction (TAC) model is widely used to reproduce pressure overload-induced HF in experimental studies, effectively inducing hypertrophy and fibrosis analogous to clinical HF [13]. Despite advances in therapeutic approaches, the persistently high morbidity and mortality of HF highlight the urgent need for novel therapeutic targets [14]. Our findings highlight the critical role of Tff3 in HF pathogenesis. We demonstrate that Tff3 expression is significantly upregulated in HF models and that its knockdown alleviates cardiac hypertrophy and fibrosis, suggesting that Tff3 may represent a promising therapeutic target in HF.

Cardiac hypertrophy and fibrosis are key features of HF that compromise myocardial function. Although hypertrophy initially serves as a compensatory response to increased hemodynamic burden, it ultimately becomes maladaptive, leading to pathological remodeling and reduced contractility [15]. Fibrosis, marked by excessive extracellular matrix deposition, stiffens the myocardium and exacerbates ventricular function [16]. Autophagy, a conserved cellular degradation pathway, plays a pivotal role in maintaining cardiac homeostasis through the clearance of damaged organelles and misfolded proteins [17]. In our study, Tff3 was markedly upregulated in TAC-induced HF models. Silencing of Tff3 significantly attenuated cardiac hypertrophy and fibrosis, as evidenced by reduced heart

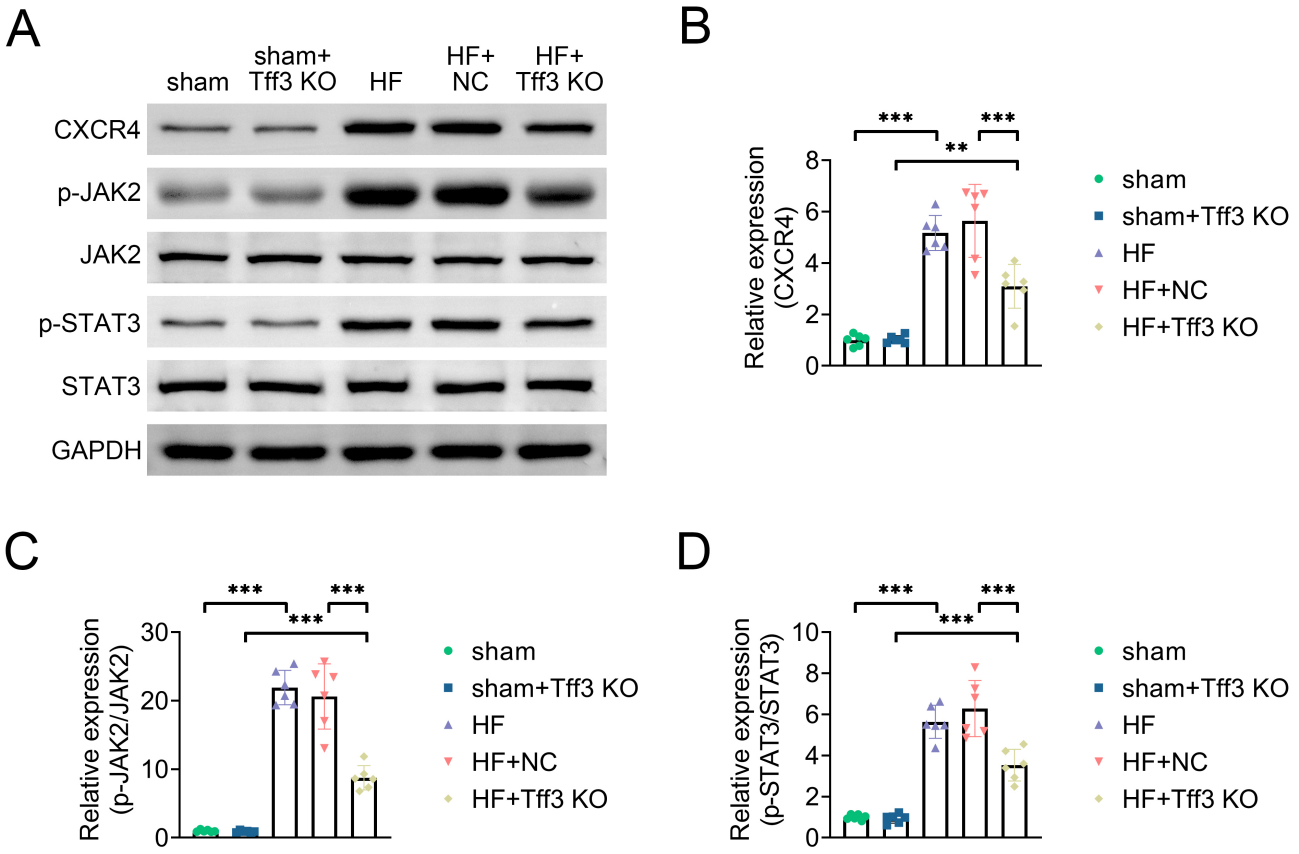

Fig. 4. Silencing of Tff3 modulates the CXCR4/JAK/STAT signaling pathway. (A) Immunoblot analysis of CXCR4, p-JAK2, JAK2, p-STAT3, and STAT3 in sham, sham + Tff3 KO, HF, HF + NC, and HF + Tff3 KO groups. GAPDH served as the loading control. (B–D) Quantification of relative CXCR4, p-JAK2/JAK2, and p-STAT3/STAT3 expression levels is shown on the right. n = 6 per group. Data are presented as mean ± SD. $^{**}p < 0.01$, $^{***}p < 0.001$. Abbreviations: NC, negative control; KO, knockout.

weight, left ventricular diameter, and fibrosis area. Furthermore, Tff3 knockdown enhanced autophagic activity, evidenced by an elevated LC3II/I ratio and reduced p62 expression, highlighting the protective role of autophagy in mitigating HF progression.

Tff3, a member of the trefoil factor family, is a small secreted peptide primarily known for its role in mucosal defense and epithelial repair [18,19]. It facilitates epithelial cell migration and wound healing and has been implicated in diverse pathological conditions, including chronic inflammation and cancer [20]. Tff3 regulates several cellular processes, such as apoptosis and autophagy, and modulates multiple signaling pathways, including NF-κB and COX2, influencing inflammation and cellular proliferation [21]. Dysregulated Tff3 expression has been associated with diseases like prostate cancer, where Tff3 overexpression suppresses apoptosis and promotes tumor growth. In liver disease, Tff3 deficiency protects against lipid accumulation, underscoring its tissue-specific effects [22]. Consistent with these findings, our results demonstrate that Tff3 knockdown enhances autophagy and reduces fibrosis in HF models, indicating its potential as a novel therapeutic target in cardiovascular diseases.

The trefoil factor family, including Tff3, is pivotal in cardiovascular physiology and pathology [23]. In this study, we observed a significant upregulation of Tff3 in heart failure and demonstrated that its knockdown alleviates cardiac hypertrophy and fibrosis. This protective effect is mediated through enhanced autophagy, which facilitates the clearance of damaged cellular components and mitigates pathological remodeling. The reduction in fibrosis and hypertrophy upon Tff3 knockdown underscores its potential to preserve cardiac function and slow HF progression. These findings indicate that targeting Tff3 could provide novel therapeutic strategies for HF and other related cardiovascular disorders.

The CXCR4/JAK/STAT pathway plays a critical role in regulating inflammation, cell survival, and autophagy [24]. CXCR4, a chemokine receptor, activates the JAK/STAT signaling pathway, leading to transcriptional changes that promote cell survival and inflammation [25]. In HF, dysregulation of this pathway contributes to maladaptive remodeling and impaired cardiac function [26]. Our findings show that Tff3 knockdown suppresses the CXCR4/JAK/STAT axis, resulting in increased autophagy and reduced fibrosis and hypertrophy. This suppression

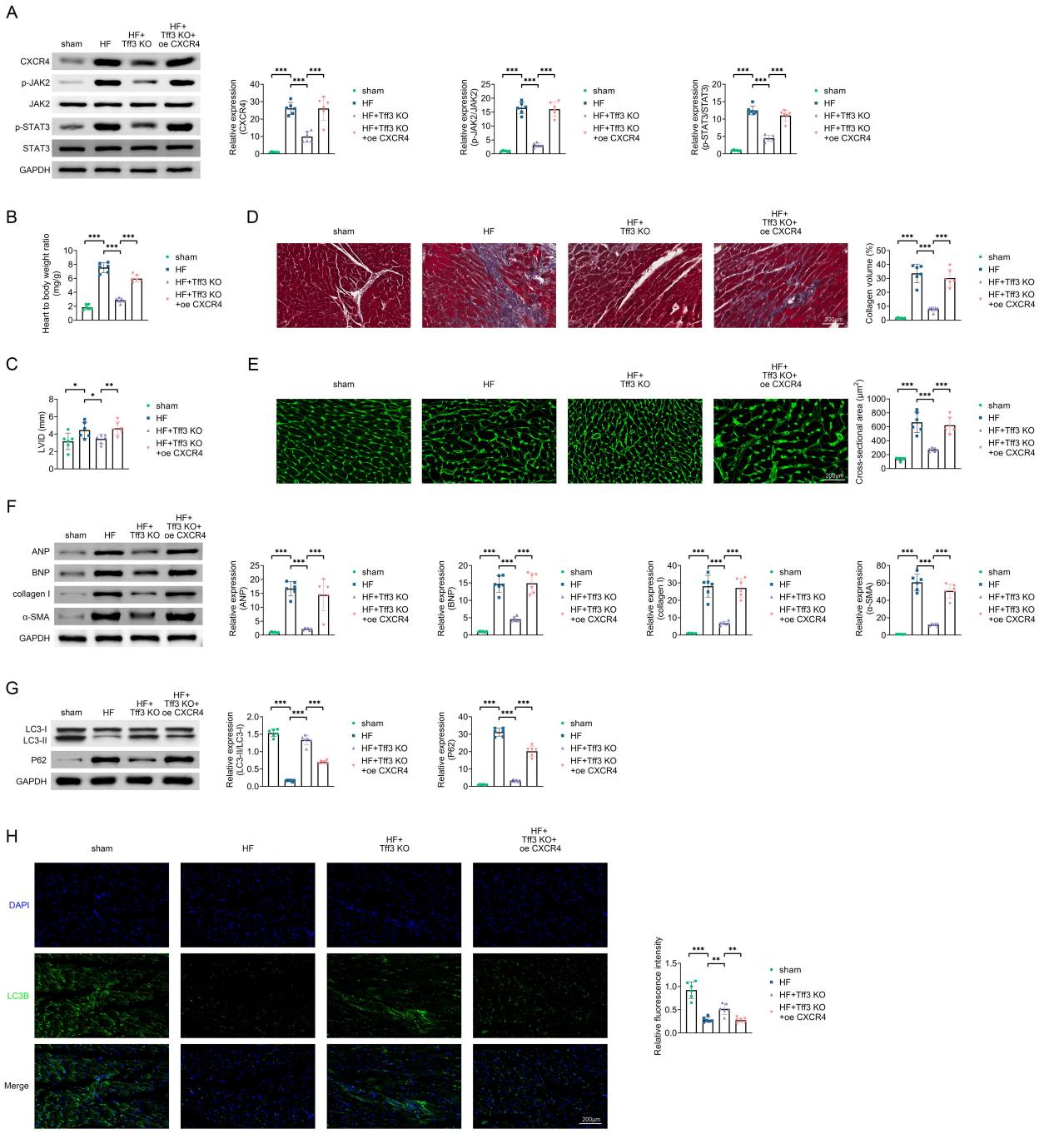

Fig. 5. Knockdown of Tff3 exerts cardioprotective effects through regulation of the CXCR4/JAK/STAT pathway. (A) Immunoblot analysis of CXCR4, p-JAK, JAK, p-STAT, and STAT expression in HF, HF + Tff3 KO, and HF + Tff3 KO + CXCR4 overexpression (OE) groups. (B) Heart-to-body weight ratio in HF, HF + Tff3 KO, and HF + Tff3 KO + CXCR4 OE groups. (C) Left ventricular internal diameter (LVID) in HF, HF + Tff3 KO, and HF + Tff3 KO + CXCR4 OE groups. (D) Masson's trichrome staining of cardiac tissue sections in HF, HF + Tff3 KO, and HF + Tff3 KO + CXCR4 OE groups, showing reduced fibrosis in the HF + Tff3 KO group (scale bar = 200 μm). (E) Wheat germ agglutinin (WGA) staining of cardiac tissue sections from HF, HF + Tff3 KO, and HF + Tff3 KO + CXCR4 OE groups, showing reduced cardiomyocyte cross-sectional area in the HF + Tff3 KO group (scale bar = 20 μm). (F) Immunoblot analysis of ANP, BNP, collagen I, and α-SMA expression levels in HF, HF + Tff3 KO, and HF + Tff3 KO + CXCR4 OE groups. GAPDH served as the loading control. (G) Immunoblot analysis of LC3-I, LC3-II, and P62 expression levels in HF, HF + Tff3 KO, and HF + Tff3 KO + CXCR4 OE groups. GAPDH served as the loading control. (H) Immunofluorescence staining of LC3B (green) and DAPI (blue) in cardiac tissue sections from HF, HF + Tff3 KO, and HF + Tff3 KO + CXCR4 OE groups, showing increased LC3B puncta in the HF + Tff3 KO group (scale bar = 200 μm). n = 6 per group. Data are presented as mean ± SD. *$p < 0.05$, **$p < 0.01$, ***$p < 0.001$. Abbreviations: NC, negative control; KO, knockout.

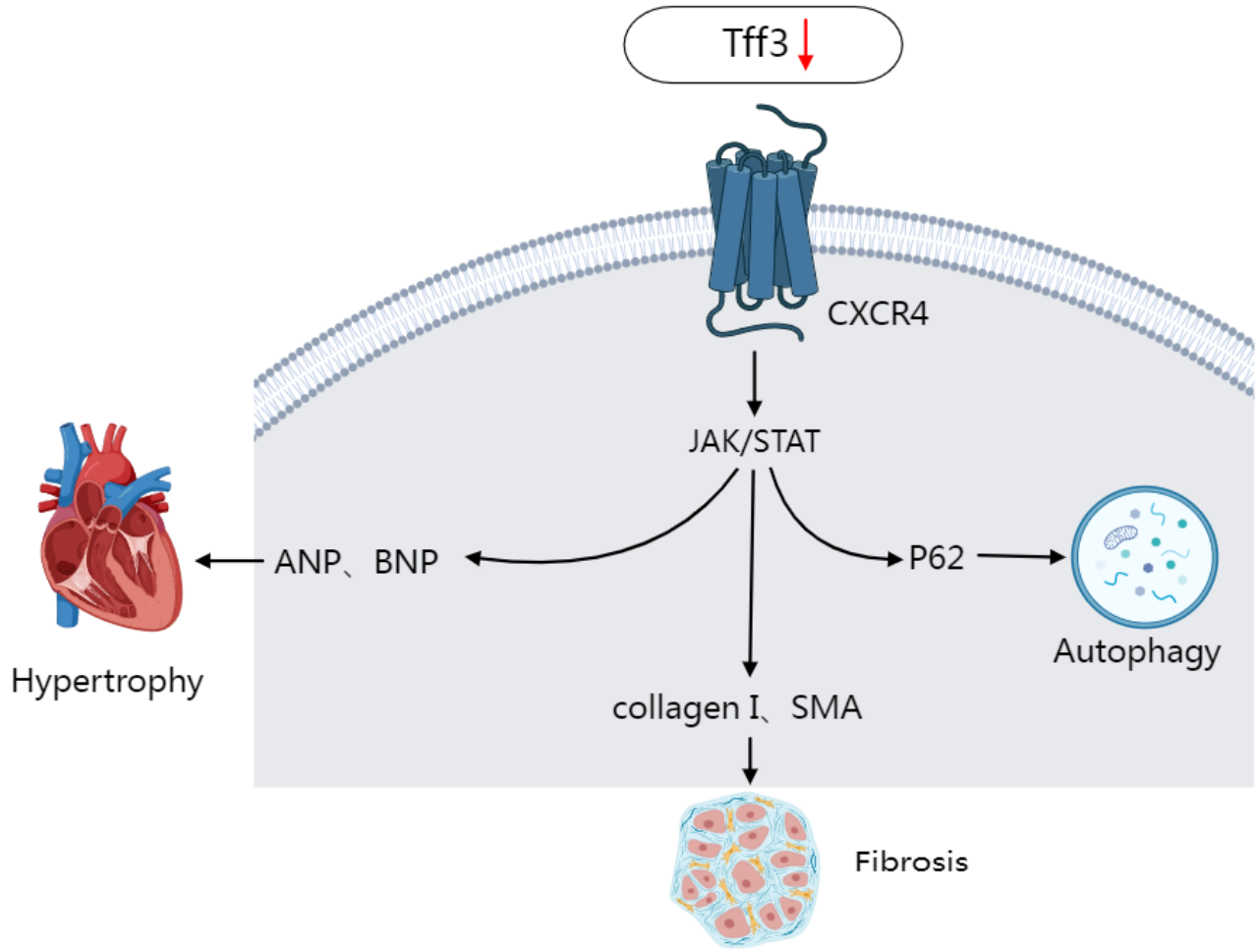

Fig. 6. Schematic summary. Tff3 significantly contributes to HF progression by modulating autophagy and the CXCR4/JAK/STAT signaling pathway. Knockdown of Tff3 alleviates cardiac hypertrophy and fibrosis, supporting its potential as a therapeutic target. Drawing software: Medpeer (https://user.medpeer.cn/).

alleviates HF symptoms by enhancing cellular clearance mechanisms and attenuating pathological signaling. Understanding Tff3's influence on this pathway provides new insights into its therapeutic potential for HF progression.

Interestingly, although CXCR4 expression was elevated following Tff3 depletion, phosphorylation levels of JAK2 and STAT3 were markedly reduced. This paradoxical observation suggests the involvement of a non-canonical regulatory mechanism, in which CXCR4 upregulation does not directly trigger downstream activation due to receptor desensitization, altered cellular localization, or compensatory signaling. This divergence highlights the complexity of the CXCR4/JAK/STAT axis under pathological stress and warrants further investigation into the underlying molecular mechanisms.

Despite these promising findings, our study has limitations that warrant further investigation. The precise molecular mechanisms by which Tff3 regulates the CXCR4/JAK/STAT pathway and autophagy remain to be fully elucidated [27]. Although the TAC model reliably mimics pressure overload-induced heart failure, it does not capture the full spectrum of pathophysiological features observed in human HF. Future studies should therefore examine Tff3's role in alternative HF models and clinical specimens. Investigating potential interactions between Tff3 and other signaling pathways could provide a more comprehensive understanding of its functions. Long-term studies are also necessary to evaluate both the therapeutic potential and safety of targeting Tff3 in HF. Moreover, additional *in vitro* experiments would yield deeper mechanistic insight and strengthen the conclusions derived from our *in vivo* observations.

Conclusion

In conclusion, our study demonstrates that Tff3 plays a critical role in the progression of HF by modulating autophagy and the CXCR4/JAK/STAT signaling pathway. Knockdown of Tff3 alleviates cardiac hypertrophy and fibrosis, highlighting its therapeutic potential (Fig. 6). These

findings contribute to a deeper understanding of the molecular mechanisms underlying HF and underscore the importance of identifying novel targets for improved therapeutic intervention. Targeting Tff3 could provide new strategies for managing HF and ultimately improving patients' quality of life.

Availability of Data and Materials

The authors declare that all data supporting the findings of this study are available within the paper and any raw data can be obtained from the corresponding author upon request.

Author Contributions

JL and YL designed the study and carried them out. JL, YL, and HL supervised the data collection. ZW designed the conception, JL, YL, and HL analyzed the data. JL, YL, and HL interpreted the data. JL drafted the manuscript. All authors contributed to important editorial changes in the manuscript. All authors read and approved the final manuscript. All authors have participated sufficiently in the work and agreed to be accountable for all aspects of the work.

Ethics Approval and Consent to Participate

Ethical approval was obtained from the Ethics Committee of The Affiliated Huai'an No.1 People's Hospital of Nanjing Medical University (Approval No. 2023-117).

Acknowledgment

Not applicable.

Funding

This research received no external funding.

Conflict of Interest

The authors declare no conflict of interest. Fig. 6 was created using Medpeer. The authors have no financial or personal relationship with Medpeer, and the use of this tool does not imply any endorsement.

References

[1] Beadle RM, Williams LK, Kuehl M, Bowater S, Abozguia K, Leyva F, *et al*. Improvement in cardiac energetics by perhexiline in heart failure due to dilated cardiomyopathy. JACC. Heart Failure. 2015; 3: 202–211. https://doi.org/10.1016/j.jchf.2014.09.009.

[2] Utter MS, Ryba DM, Li BH, Wolska BM, Solaro RJ. Omecamtiv Mecarbil, a Cardiac Myosin Activator, Increases Ca2+ Sensitivity in Myofilaments With a Dilated Cardiomyopathy Mutant Tropomyosin E54K. Journal of Cardiovascular Pharmacology. 2015; 66: 347–353. https://doi.org/10.1097/FJC.0000000000000286.

[3] Sharov VG, Goussev A, Lesch M, Goldstein S, Sabbah HN. Abnormal mitochondrial function in myocardium of dogs with chronic heart failure. Journal of Molecular and Cellular Cardiology. 1998; 30: 1757–1762. https://doi.org/10.1006/jmcc.1998.0739.

[4] Šešelja K, Bazina I, Vrecl M, Farger J, Schicht M, Paulsen F, *et al*. Tff3 Deficiency Differentially Affects the Morphology of Male and Female Intestines in a Long-Term High-Fat-Diet-Fed Mouse Model. International Journal of Molecular Sciences. 2023; 24: 16342. https://doi.org/10.3390/ijms242216342.

[5] Šešelja K, Bazina I, Vrecl M, Welss J, Schicht M, Mihalj M, *et al*. Tff3 Deficiency Protects against Hepatic Fat Accumulation after Prolonged High-Fat Diet. Life (Basel, Switzerland). 2022; 12: 1288. https://doi.org/10.3390/life12081288.

[6] Mihalj M, Bujak M, Butković J, Zubčić Ž, Tolušić Levak M, Čes J, *et al*. Differential Expression of *TFF1* and *TFF3* in Patients Suffering from Chronic Rhinosinusitis with Nasal Polyposis. International Journal of Molecular Sciences. 2019; 20: 5461. https://doi.org/10.3390/ijms20215461.

[7] Yang L, Zhang X, Zhang J, Liu Y, Ji T, Mou J, *et al*. Low expression of *TFF3* in papillary thyroid carcinoma may correlate with poor prognosis but high immune cell infiltration. Future Oncology (London, England). 2022; 18: 333–348. https://doi.org/10.2217/fon-2020-1183.

[8] Hormdee D, Prajaneh S, Kampichai A, Tak R, Chaiyarit P. Prolonged Suppressive Effects of Periodontitis on Salivary TFF3 Production. European Journal of Dentistry. 2019; 13: 193–198. https://doi.org/10.1055/s-0039-1693949.

[9] Lee SI, Kim IH. Nucleotide-mediated SPDEF modulates TFF3-mediated wound healing and intestinal barrier function during the weaning process. Scientific Reports. 2018; 8: 4827. https://doi.org/10.1038/s41598-018-23218-4.

[10] Šešelja K, Bazina I, Welss J, Schicht M, Paulsen F, Bijelić N, *et al*. Effect of Tff3 Deficiency and ER Stress in the Liver. International Journal of Molecular Sciences. 2019; 20: 4389. https://doi.org/10.3390/ijms20184389.

[11] Rennison JH, McElfresh TA, Okere IC, Patel HV, Foster AB, Patel KK, *et al*. Enhanced acyl-CoA dehydrogenase activity is associated with improved mitochondrial and contractile function in heart failure. Cardiovascular Research. 2008; 79: 331–340. https://doi.org/10.1093/cvr/cvn066.

[12] Parodi-Rullan R, Barreto-Torres G, Ruiz L, Casasnovas J, Javadov S. Direct renin inhibition exerts an anti-hypertrophic effect associated with improved mitochondrial function in post-infarction heart failure in diabetic rats. Cellular Physiology and Biochemistry: International Journal of Experimental Cellular Physiology, Biochemistry, and Pharmacology. 2012; 29: 841–850. https://doi.org/10.1159/000178526.

[13] Osterholt M, Nguyen TD, Schwarzer M, Doenst T. Alterations in mitochondrial function in cardiac hypertrophy and heart failure. Heart Failure Reviews. 2013; 18: 645–656. https://doi.org/10.1007/s10741-012-9346-7.

[14] Lee SH, Doliba N, Osbakken M, Oz M, Mancini D. Improvement of myocardial mitochondrial function after hemodynamic support with left ventricular assist devices in patients with heart failure. The Journal of Thoracic and Cardiovascular Surgery. 1998; 116: 344–349. https://doi.org/10.1016/s0022-5223(98)70136-9.

[15] Yusufu A, Shayimu P, Tuerdi R, Fang C, Wang F, Wang H. TFF3 and TFF1 expression levels are elevated in colorectal cancer and promote the malignant behavior of colon cancer by activating the EMT process. International Journal of Oncology. 2019; 55: 789–804. https://doi.org/10.3892/ijo.2019.4854.

[16] Shukla A, Gupta P, Singh R, Mishra DP. Glycolytic inhibitor 2-Deoxy-d-Glucose activates migration and invasion in glioblas-

toma cells through modulation of the miR-7-5p/TFF3 signaling pathway. Biochemical and Biophysical Research Communications. 2018; 499: 829–835. https://doi.org/10.1016/j.bbrc.2018.04.001.

[17] Liu J, Kim SY, Shin S, Jung SH, Yim SH, Lee JY, *et al*. Overexpression of TFF3 is involved in prostate carcinogenesis via blocking mitochondria-mediated apoptosis. Experimental & Molecular Medicine. 2018; 50: 1–11. https://doi.org/10.1038/s12276-018-0137-7.

[18] Houben T, Harder S, Schlüter H, Kalbacher H, Hoffmann W. Different Forms of TFF3 in the Human Saliva: Heterodimerization with IgG Fc Binding Protein (FCGBP). International Journal of Molecular Sciences. 2019; 20: 5000. https://doi.org/10.3390/ijms20205000.

[19] Wu S, Kit V, In J, Kinjo S. Paraspinal regional analgesic techniques in spine surgery−a narrative review. Signa Vitae. 2023; 19: 9–15. https://doi.org/10.22514/sv.2023.068.

[20] Timofte AD, Giuşcă SE, Lozneanu L, Manole MB, Prutianu I, Gafton B, *et al*. HOXB13 and TFF3 can contribute to the prognostic stratification of prostate adenocarcinoma. Romanian Journal of Morphology and Embryology. 2021; 62: 41–52. https://doi.org/10.47162/RJME.62.1.04.

[21] Shen M, Yang L, Lei T, Zhang P, Xiao L, Cao S, *et al*. Correlation between CA12 and TFF3 and their prediction value of neoadjuvant chemotherapy response in breast cancer. Journal of Clinical Pharmacy and Therapeutics. 2022; 47: 609–618. https://doi.org/10.1111/jcpt.13580.

[22] Paterson AL, Gehrung M, Fitzgerald RC, O'Donovan M. Role of TFF3 as an adjunct in the diagnosis of Barrett's esophagus using a minimally invasive esophageal sampling device-The Cytosponge™. Diagnostic Cytopathology. 2020; 48: 253–264. https://doi.org/10.1002/dc.24354.

[23] Liu J, Yang Q, Chen Z, Lv S, Tang J, Xing Z, *et al*. TFF3 mediates the NF-κB/COX2 pathway to regulate PMN-MDSCs activation and protect against necrotizing enterocolitis. European Journal of Immunology. 2021; 51: 1110–1125. https://doi.org/10.1002/eji.202048768.

[24] Wei H, Chen F, Chen J, Lin H, Wang S, Wang Y, *et al*. Mesenchymal Stem Cell Derived Exosomes as Nanodrug Carrier of Doxorubicin for Targeted Osteosarcoma Therapy via SDF1-CXCR4 Axis. International Journal of Nanomedicine. 2022; 17: 3483–3495. https://doi.org/10.2147/IJN.S372851.

[25] Xiao S, Zhang D, Liu Z, Jin W, Huang G, Wei Z, *et al*. Diabetes-induced glucolipotoxicity impairs wound healing ability of adipose-derived stem cells-through the miR-1248/CITED2/HIF-1α pathway. Aging. 2020; 12: 6947–6965. https://doi.org/10.18632/aging.103053.

[26] Larocca TJ, Jeong D, Kohlbrenner E, Lee A, Chen J, Hajjar RJ, *et al*. CXCR4 gene transfer prevents pressure overload induced heart failure. Journal of Molecular and Cellular Cardiology. 2012; 53: 223–232. https://doi.org/10.1016/j.yjmcc.2012.05.016.

[27] Li J, Yu T, Sun J, Zeng Z, Liu Z, Ma M, *et al*. Comprehensive analysis of cuproptosis-related immune biomarker signature to enhance prognostic accuracy in gastric cancer. Aging. 2023; 15: 2772–2796. https://doi.org/10.18632/aging.204646.